

Effect of red mud and cenosphere reinforcements on the structural and emi shielding performance of open-cell aluminum foams

Ashutosh Pandey¹, D. P. Mondal¹, Raghvendra Khedle¹, and Mayur Kumar Rajak^{2*}

¹Department of Mechanical Engineering, Technocrats Institute of Technology, Bhopal, Madhya Pradesh, India

²School of Mechanical Engineering, VIT Bhopal University, Sehore, Madhya Pradesh, India

Abstract. The Open-cell Al foam (OCAF) with an average density of 0.12 g/cc were synthesized successfully through reticulation technique, using polyurethane (PU) foam as a precursor. For further enhancing the multifunctional properties of OCAF, here in this work it is reinforced with red mud and cenospheres. The addition of red mud and cenosphere reinforcements in OCAF at 10% by weight is studied to analyze their effect on microstructure, mechanical strength and electromagnetic wave (EMW) absorption of the foam. The EMW absorption was evaluated using a Vector network analyzer in X-Band (i.e. 8.2 -12.4 GHz) frequency range. OCAF with cenosphere shows the highest total shielding effectiveness (~28 dB) which is then followed by red mud reinforcement and bare OCAF. In cenosphere, absorption component dominates the total shielding. Whereas in red mud, reflection and absorption contribute almost equally in total shielding. This reinforcement also enhances the compressive strength and energy absorption of the OCAF structure. The result demonstrated the use of cenosphere and red mud to tailor the properties of OCAF in terms of EMW absorption and structure application for the development of new material for electromagnetic shielding.

1. Introduction

In the modern era, almost every aspect of human life is surrounded by electronic devices and systems that rely on electromagnetic (EM) signal transmission and processing [1, 2]. Mobile phones, televisions, the Internet of Things (IoT), telecommunication networks, and countless other technologies function through the generation and reception of electromagnetic waves. In fact, the entire universe is continuously immersed in electromagnetic radiation of varying frequencies and amplitudes [3]. While this invisible web of EM waves has enabled remarkable technological advancement, it has also introduced significant challenges. One such challenge is electromagnetic interference (EMI), which arises when unintended electromagnetic signals disrupt the operation of nearby electronic equipment [4, 5]. This interference can degrade device performance, distort signal transmission, and in severe cases, cause complete malfunction [6]. Beyond the technical domain, continuous exposure to electromagnetic radiation has also raised growing concerns about its potential impact on human health. Consequently, there is an increasing global emphasis on developing materials that can effectively shield electromagnetic radiation to ensure both device reliability and environmental safety [7, 8].

Electromagnetic shielding materials function primarily through two mechanisms—reflection and absorption of electromagnetic waves [9, 10]. Reflection-based shielding is generally achieved using electrically conductive materials, such as metals, which reflect incoming EM waves at their surfaces. This mechanism is desirable for applications like antennas and communication systems, where signal redirection or confinement is required. In contrast, absorption-dominated shielding materials are more suitable for stealth technologies in defense applications, where it is essential to suppress or attenuate reflected signals to avoid detection. Among various metals, aluminum has emerged as a promising EMI shielding material due to its high electrical conductivity, low density, corrosion resistance, and ease of processing [11, 12]. However, when aluminum is converted into a porous or open-cell foam structure, its shielding behavior changes significantly [13, 14]. The porous architecture introduces a large number of internal surfaces, interfaces, and voids that act as scattering centers for the incoming EM waves. These multiple reflections and scatterings within the interconnected pore network enhance the probability of wave attenuation through absorption, thereby transforming a typically reflective metal into a hybrid absorber–reflector material [14].

* Corresponding author: smecvisitinhfaculty@vitbhopal.ac.in, rajakmayur@gmail.com

Furthermore, the incorporation of ceramic or mineral reinforcements within the aluminum matrix can further modify its electromagnetic and mechanical responses [15, 16]. Reinforcements such as red mud (an industrial byproduct of alumina production) and fly ash or cenospheres (derived from coal combustion) contain phases that are both magnetic and dielectric in nature [17, 18]. The presence of these reinforcements within the metallic foam introduces additional interfacial boundaries, enhances polarization losses, and contributes to multiple scattering and magnetic-dielectric coupling effects—all of which are favorable for EMI absorption.

In this context, the present study focuses on the synthesis and characterization of open-cell aluminum foams with and without reinforcements of red mud and cenosphere particles. The novelty of this work lies in the use of industrial waste as a reinforcement in OCAF lightweight structure for high energy absorption and electromagnetic shielding. The primary objective is to examine how the inclusion of these industrial waste-derived reinforcements influences the microstructure, mechanical compression behavior, and electromagnetic shielding effectiveness (SE) of the foams. The study aims to establish a relationship between the structural features, phase composition, and EMI shielding mechanisms (reflection, absorption, and total SE) to assess the suitability of these lightweight composite foams for potential stealth and communication applications. The main challenge involved during the synthesis of this foam is to maintain the uniformity of the reinforcing particles and maintain the structural integrity during sintering of the foam. Here we have compared the properties of three different types of OCAF that is (i) bare Al foam which is denoted by Al, (ii) Al foam with 10% by weight of cenosphere, denoted by Al-CN, and (iii) Al foam with 10% by weight of red mud, denoted by Al-RM.

2. Experimental

2.1 Raw Materials and Foam making

Commercially pure aluminum powder (99.5% purity) with an average particle size of approximately 25 μm (325 mesh) was used as the base material (Figure 1(c)). The cenospheres, obtained from coal fly ash, had a spherical morphology with an average particle size of about 30 μm (Figure 1(a)). The red mud, a by-product of the Bayer alumina extraction process, was used in powder form after drying and sieving to below 45 μm (Figure 1(b)). Both red mud and cenosphere were used as reinforcements at 5 wt% of the total aluminum powder weight. All powders were used in the as-received condition after drying at 120 $^{\circ}\text{C}$ to remove moisture.

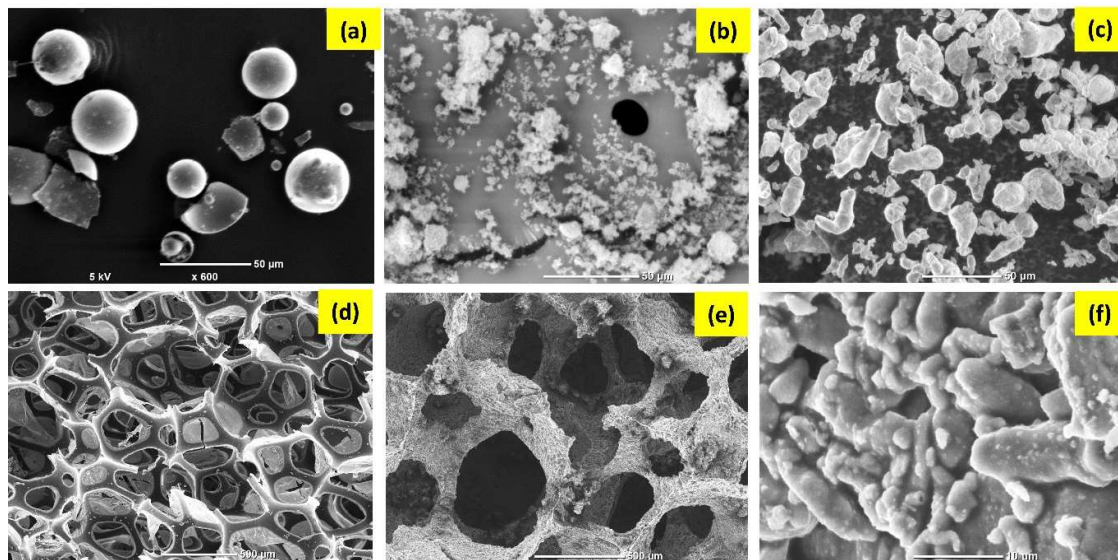


Fig. 1. (a) microstructure of cenosphere, (b) redmud powder, (c) Pure Al powder, (d) 50 PPI PU foam template, (e) OCAF with pores and cell wall, and (f) Diffusion bonding of Al particles during sintering.

A polyurethane (PU) foam with a pore density of 50 pores per inch (PPI) (Figure 1(d)) was selected as the sacrificial template to produce the open-cell structure. An acetone-based 5 wt% phenolic resin solution was employed as the binder medium for slurry preparation and coating, providing uniform distribution and adequate green strength before sintering. The foams were prepared by adopting a replica (template) technique, which has been widely reported for producing metallic foams with controlled pore structures [13]. Initially, 100 g of aluminum powder was dispersed in 100 mL of acetone-based phenolic resin solution to form a homogeneous slurry. The mixture was stirred for approximately 30 minutes using a magnetic stirrer to ensure uniform dispersion

of the metallic particles. In the case of composite foams, the desired reinforcement (red mud or cenosphere) was first mixed with the aluminum powder at a ratio of 5 wt%, followed by the same slurry preparation procedure. The PU foam templates were immersed into the aluminum slurry to ensure complete infiltration of the coating throughout the pore network. After dipping, each foam was gently rolled between rubber rollers to remove excess slurry and promote uniform distribution of particles within the foam skeleton. This dipping and rolling process was repeated four to five times to achieve a consistent coating thickness on all internal ligaments of the foam.

The impregnated foams were then dried in a vacuum oven at 150 °C for 4 hours, allowing complete evaporation of the solvent and partial curing of the resin binder. The dried green foams were subsequently subjected to a thermal decomposition step to remove the PU template. The heating was carried out gradually up to 400 °C, with a dwell time of 1 hour, to ensure complete burnout of the polymer skeleton without collapsing the metallic network. Finally, the foams were sintered at 660 °C for 1 hour under vacuum (10^{-4} mbar) to promote metallurgical bonding between the aluminum particles and to obtain a mechanically stable open-cell structure. The sintered foams retained the three-dimensional interconnected network of the original PU template, forming a lightweight metallic architecture suitable for structural and electromagnetic applications.

2.2 Characterization

The raw materials are characterized for their particle size distribution and shape using SEM micrographs. The XRD pattern of red mud, cenosphere and aluminium particles were studied using Rigaku miniflex (Model-600) X-ray diffractometer at scan rate of 0.2°/sec and Cu-K α radiation. The compressive strength of the foam samples were measured using Instron UTM (model:8801) at a strain rate 0.01/s. The density of the foam sample was measured from the weight and volume of the samples. EMI shielding tests was carried out using Keysight vector network analyzer (Model:- E5080B) in X-band frequency. For this test sample of dimension 10 mm width, 22.5 mm length and 5 mm thickness were used. During the tests scattering parameters (i.e. S11 and S21) were recorded and through which the total shielding effectiveness was calculated based on the mathematical relations reported elsewhere [19, 20].

3. Results and discussion

3.1 Morphology and Phase Analysis of Raw Materials

The morphology of the raw materials used for the fabrication of open-cell aluminum foams is illustrated in Figure 1. The cenosphere particles (Figure 1 (a)) were observed to be spherical and hollow in nature, with an average particle size of approximately 30 μm . These hollow spheres, also referred to as microballoons, are characterized by thin outer shells, which could be clearly seen in some of the fractured or crushed particles. In contrast, the red mud particles (Figure 1(b)) exhibited a dense, angular morphology with a relatively finer particle size of around 40 μm . The aluminum particles (Figure 1(c)) appeared irregular in shape and were comparatively coarser, with an average particle size close to 30 μm . Overall, the morphology of these powders suggests that while the aluminum and red mud particles contribute to the density and mechanical integrity of the composite, the hollow structure of the cenospheres is expected to reduce the overall weight and increase porosity in the final foam.

For the confirmation of the materials and its purity, X-ray diffraction (XRD) was carried out for the redmud, cenosphere and Al powder used for the synthesis of OCAF. The diffraction pattern of different material is mentioned in Figure 2. Figure 2(a) shows the XRD pattern of cenosphere, the presence of mullite ($3\text{Al}_2\text{O}_3 \cdot 2\text{SiO}_2$), sillimanite (Al_2SiO_5), ferrosilicate, quartz, and graphitic carbon at their respective position confirms the material and its purity. The presence of these compounds shows that cenosphere have different ceramic and semi-conductive phases which can help in increasing the shielding properties of the OCAF structure. Same kind of properties are also found in red mud. Figure 2(b) shows the scan pattern of red mud, the presence of different compounds i.e. calcium carbonate (CaCO_3), calcium aluminosilicate ($\text{Ca}_3\text{Al}_2\text{SiO}_4$), hematite (Fe_2O_3), quartz (SiO_2), aluminum oxide (Al_2O_3), and titanium dioxide (TiO_2) confirms the material also no any other presence of peak confirms the purity of the materials. Whereas for Al powder the XRD graph only shows the four identical peaks of the Al which confirm its presence and purity.

The morphological study was done through SEM. The microstructural analysis of bare and reinforced OCAF is shown in Figure 1 (e and f). From Figure 1(e), it is found that the synthesized OCAF have fully open inter connected pores with average strut size of 200 μm , owing to the replication of PU foam used as a template. In case of cenosphere and red mud reinforced OCAFs (i.e. Al-CN and Al-RM), the particles get uniformly distributed through the foam structures and incorporated the multiple interfaces inside the material which may help in increase the total EMI shielding properties of the foam. In the Al-CN foam, hollow cenosphere particles are evenly dispersed within the aluminum ligaments. Their intact spherical morphology increases internal porosity and interfacial area, reducing overall density and promoting multiple scattering of electromagnetic waves. The compositional difference between red mud and cenosphere—ceramic versus silicate-rich hollow spheres—is expected to distinctly influence the mechanical and EMI shielding behavior of the foams.

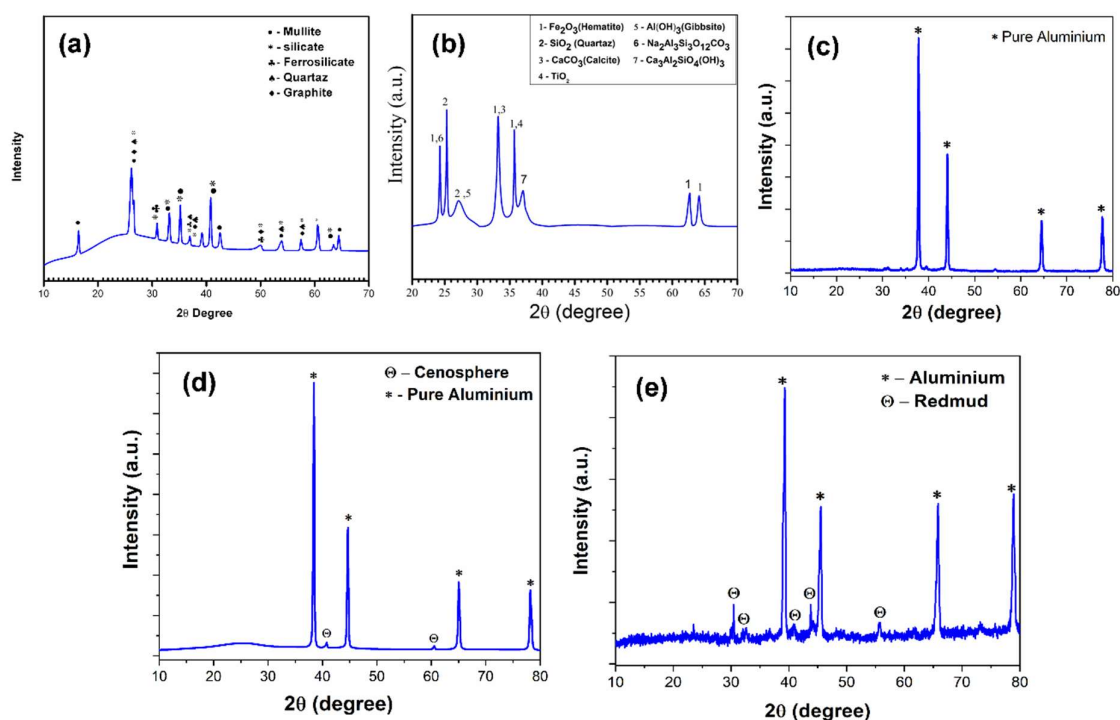


Fig. 2. XRD graph of (a) cenosphere, (b) redmud, (c) pure Al powder, (d) Sintered Al-CN foam, and (e) Sintered Al-RM foam.

3.2 Mechanical Behavior

The density of the pure open-cell aluminum foam (OCAF) was measured as $45 \pm 0.5 \text{ g/cm}^3$, whereas the Al-CN and Al-RM foams exhibited densities of $42 \pm 0.5 \text{ g/cm}^3$ and $47 \pm 0.5 \text{ g/cm}^3$, respectively. The cenosphere-reinforced foam was slightly lighter due to the low intrinsic density of cenospheres ($\sim 0.65 \text{ g/cm}^3$), while the red mud-reinforced foam was marginally heavier owing to the higher density of red mud ($\sim 3.2 \text{ g/cm}^3$). However, the overall difference in density among the foams remained small. The compressive stress-strain curves for all foams are shown in Figure 3(a). Each curve follows the typical behavior of open-cell metallic foams, consisting of an initial linear elastic region, a plateau region characterized by cell collapse, and a densification region, where stress rises sharply with increasing strain. The other key parameters that are calculated using stress-strain curve are plateau stress, densification strain and energy absorption capacity of the foam. For energy absorption, the area under the curve up to densification strain is considered.

From Figure 3(a), it is observed that the Al-CN foam has the highest plateau stress (5.5 MPa), which is then followed by Al-RM (i.e., 2.8 MPa) and Al (i.e., 2.1 MPa) foam. The energy absorption calculated from the stress-strain graph also follows the same trend, which is 2.78 MJ/m^3 , 1.6 MJ/m^3 , and 1.2 MJ/m^3 for Al-CN, Al-RM, and Al foam, respectively. This increase in plateau stress and energy absorption value shows the enhancement of mechanical properties with the reinforcement of cenosphere and red mud particles. The incorporation of cenosphere particles significantly enhances the plateau stress (more than two-fold) and energy absorption (almost double) due to its hollow spherical shape and lesser density, which increase the reinforcing particles inside the matrix. Whereas for the same 10% wt. addition of red mud, it shows a moderate increment in strength and energy absorption as compared to pure Al foam.

3.3 Electromagnetic Shielding Effectiveness (EMI-SE)

The EMI shielding effectiveness of pure aluminum foam (Al), red mud-reinforced foam (Al-RM), and cenosphere-reinforced foam (Al-CN) is presented in Figure 3(b-d), showing the variation of absorption (SEA), reflection (SER), and total shielding effectiveness (SET) in the frequency range of 8.4–12.4 GHz. The absorption component (SEA) was found to be highest for the Al-CN foam ($\sim 28 \text{ dB}$), moderate for the pure Al foam ($\sim 21 \text{ dB}$), and lowest for the Al-RM foam ($\sim 7 \text{ dB}$). In contrast, the reflection component (SER) showed an opposite trend, with the Al-RM foam exhibiting the highest reflection ($\sim 10 \text{ dB}$), while Al-CN and Al foams showed much

lower reflection values of about 1.0–1.2 dB. Consequently, the total EMI shielding (SET) values were observed to be 28 dB for Al–CN, 20 dB for Al, and 18 dB for Al–RM.

From Figure 3(b, c, and d), it is clearly observed that in the total shielding effectiveness of the Al–CN foam, absorption is the main dominating mechanism, while the reflection component is much less. This superior property may be attributed to the presence of large interfaces in between the different ceramic phases present in cenosphere and Al. The interconnected foam structure may also help improve the foam's shielding properties. These interconnected pores with incorporated spherical cenosphere particles increase the surface area, which helps increase the multiple reflections of EMW inside the foam structure. Every time when the waves get reflected, it loses energy and ultimately helps in increasing the total shielding effectiveness of the foam. Moreover, the shell

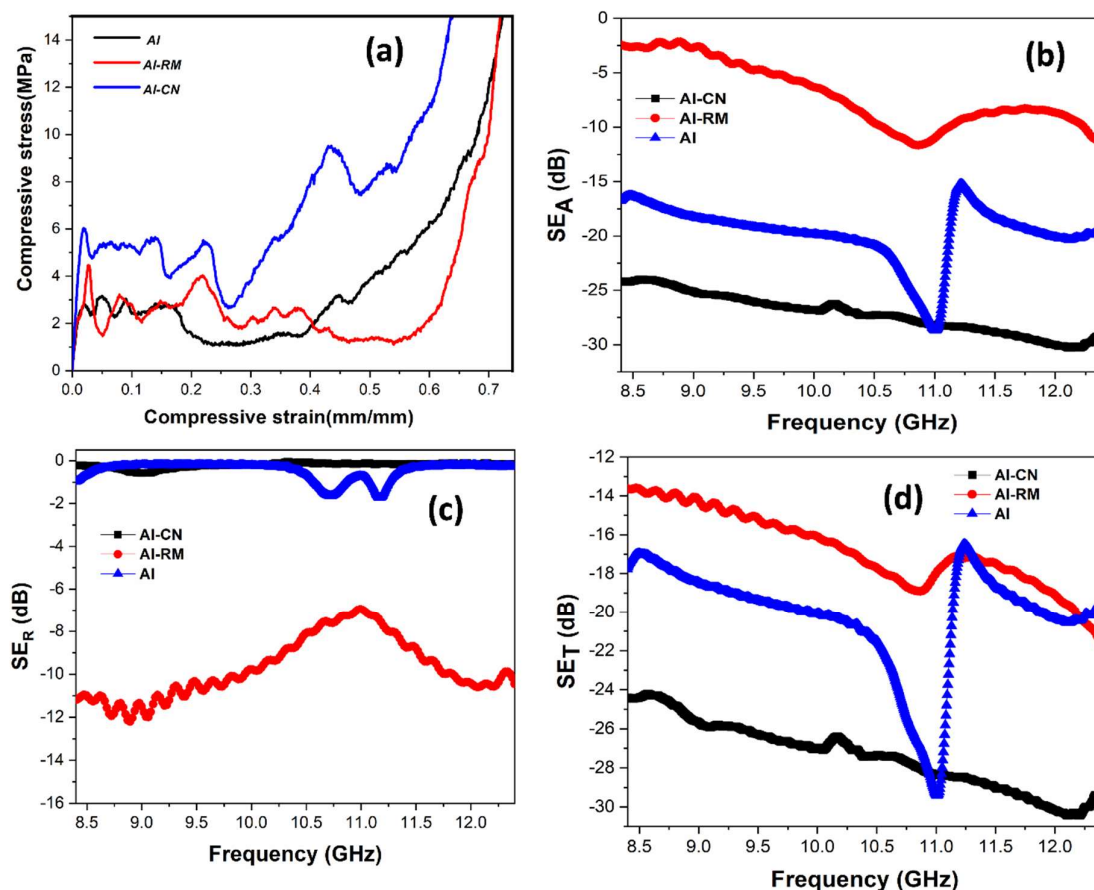


Fig. 3. (a) Compressive stress-strain graph of different OCAFs, (b) absorption component in total shielding, (c) reflection component of shielding, and (d) total shielding effectiveness.

wall thickness of cenosphere is $\sim 15 \mu\text{m}$, which allows the partial penetration of EMWs; this causes the multiple internal reflections and loss of energy inside the particles. The combination of all these mechanisms leads to enhanced overall absorption capacity of the Al–CN foam in the X-band frequency range. In the case of red mud, the particles are dense and solid and majorly consist of TiO_2 , Fe_2O_3 , and Al_2O_3 phases, which are nonmagnetic and nonconductive. Due to the high density of the material, the EMWs could not penetrate it, resulting in the reflection of the waves at the surface and a decrease in absorption. Therefore, in Al–RM foam, reflection and absorption contribute almost equally and have moderate total shielding as compared to other foams.

For the pure aluminum foam, shielding is primarily governed by surface reflection and partial absorption due to multiple scattering within its open-cell structure. During sintering, the formation of thin oxide layers on the cell walls introduces additional interfaces, slightly improving absorption but simultaneously lowering electrical conductivity. The highly open structure allows deeper penetration of EM waves, leading to repeated scattering but weaker reflection efficiency. At higher frequencies (above $\sim 11 \text{ GHz}$), the incident wavelength becomes comparable to the cell size, reducing the effectiveness of multiple scattering. Consequently, the SEA decreases slightly, while reflection becomes more pronounced—an effect also observed for the Al–RM foam. Overall, the Al–CN foam demonstrates the best EMI shielding performance due to its optimal balance

between conductivity, interfacial polarization, and structural porosity. The combination of high interface density, multiple scattering, and hollow dielectric inclusions leads to efficient attenuation of electromagnetic energy through absorption rather than reflection. Hence, the dominant shielding mechanism in Al–CN foams is absorption-driven, making them highly suitable for stealth and lightweight shielding applications.

4. Conclusions

The fully inter-connected OCAF was prepared through reticulation method using PU foam as a precursor. The pore, strut and cell structure were effectively replicated. Cenosphere and red mud were used as a reinforcement in foam structure without compromising the basic structure of the foam. The reinforcing agent enhances the mechanical and shielding properties of the foam. The Al–CN foam shows the highest plateau strength which is much higher as compared to Al–RM and Al foam, and also follows the same trend in term of energy. Due to hollow particles and lesser density of cenosphere, the reinforcement volume fraction in Al matrix is higher as compared to red mud reinforcement. Red mud reinforcement also improved strength but to a lesser extent, owing to its higher density and compact particle structure. The EMI shielding effectiveness of the foams was found to depend strongly on the reinforcement type and microstructural characteristics. The total shielding effectiveness (SET) reached approximately 28 dB for Al–CN, 20 dB for pure Al, and 18 dB for Al–RM foams in the 8.4–12.4 GHz range. The shielding in pure Al and Al–CN foams was predominantly absorption-driven, whereas in Al–RM foams, both reflection and absorption contributed almost equally. The superior absorption in Al–CN foams arise from their high interface density, increased multiple scattering, and dielectric polarization within the hollow cenospheres, while the denser red mud particles in Al–RM foams enhance reflection due to reduced porosity and higher material density.

Overall, the study demonstrates that lightweight aluminum foams reinforced with industrial waste materials such as red mud and cenospheres can effectively combine structural and functional performance. Particularly, the cenosphere-reinforced foams show excellent absorption-dominated EMI shielding, making them promising candidates for applications requiring lightweight, eco-friendly, and absorption-based electromagnetic protection materials.

References

- [1] B. Mekimah, Y. Mohamdi, S. Benatallah, Impact of the electromagnetic waves on the human health and environment: study and analysis, University Of Kasdi Merbah Ouargla, (2024).
- [2] A.E. Ubhenin, J. Isabona, F. Anura, R.I. Idris, Unraveling the impact of electromagnetic radiation on human health: A comprehensive review, African Journal of Pharmaceutical Research and Development **16** (1) 91-99 (2024).
- [3] N. Sandoval-Diez, L. Belácková, A.F. Veludo, H. Jalilian, F. Guida, I. Deltour, A. Thielens, M. Zahner, J. Fröhlich, A. Huss, Determining the relationship between mobile phone network signal strength and radiofrequency electromagnetic field exposure: protocol and pilot study to derive conversion functions, Open Research Europe **4** 206 (2025).
- [4] S.A. Hamouda, N.S. Amneenah, Electromagnetic interference impacts on electronic systems and regulations, International Journal of Advanced Multidisciplinary Research and Studies **4** (1) 124-127 (2024).
- [5] J.T. Orasugh, O.J. Botlhoko, L.T. Temane, S.S. Ray, Progress in polymer nonwoven textile materials in electromagnetic interference shielding applications, Functional Composite Materials **5** (1), 5 (2024).
- [6] K. Ramya, J. Gopalakrishnan, B. Chokkalingam, R. Verma, L. Mihet-Popa, A Complete Review of Electromagnetic Interference in Electric Vehicle, IEEE Access (2025).
- [7] N. Burdeina, L. Levchenko, I. Korduba, S. Shamanskyi, Y. Biruk, M. Dovhanovskyi, S. Zozulya, A. Klymchuk, K. Nikolaiev, D. Osadchyi, Applying Heterogeneous Building Materials For The Protection Of People Against Electromagnetic Radiation, Eastern-European Journal of Enterprise Technologies **131** (10) (2024).
- [8] Z. Wang, L. Ma, H. Ma, M. Xu, X. Wu, D. Zhang, C.B. Park, J. Wang, Double-layer electromagnetic shielding materials with microcellular structure for strong absorption and low reflection, Journal of Materials Science & Technology **245** 227-237 (2026).
- [9] Y. Shi, M. Wu, S. Ge, J. Li, A.S. Alshammari, J. Luo, M.A. Amin, H. Qiu, J. Jiang, Y.M. Asiri, Advanced functional electromagnetic shielding materials: a review based on micro-nano structure interface control of biomass cell walls, Nano-Micro Letters **17** (1), 3 (2025).
- [10] J. Liu, V. Nicolosi, Electrically insulating electromagnetic interference shielding materials: a perspective, Advanced Functional Materials **35** (18) 2407439 (2025).
- [11] A. Voronin, M. Makeev, I. Damaratsky, Aluminium Mesh Transparent Conductor with Irregular Structure as Effective EMI Shielding Material, 2024 International Ural Conference on Electrical Power Engineering (UralCon), IEEE, pp. 663-667 (2024).

- [12] C.Q. Hui, K. Ng, C. Umair, B.G.Z. Hong, Optimising Materials And Design For Effective Electromagnetic Shielding In Phone Cases.
- [13] A. Pandey, R. Kumar, D.P. Mondal, P. Kumar, S. Singh, Nickel oxide-sprinkled in-situ grown hierarchal graphitic jungle anchored feathery aluminum foam: A novel material for remarkable electromagnetic waves absorption, *Materials Today Nano* **21** 100301 (2023).
- [14] A. Pandey, R. Dubey, S.K. Srivastava, H. Jain, A. Sharma, R. Raj, S. Sriram, B.N. Yadav, V. Chilla, G.K. Gupta, R. Kumar, D.P. Mondal, Synergetic effect of reduced graphene oxide and reticulated open-cell aluminum hybrid composite foam for high-performance electromagnetic wave absorption, *Journal of Alloys and Compounds* **968**, 172065 (2023).
- [15] İ. Tekin, M. Pekgöz, The effects of ZnO powder and different fiber types used in tuff/calcite-based geopolymers on electromagnetic shielding effectiveness, *Journal of Building Engineering* **89** 109343 (2024).
- [16] M. Jahan, S. Hossain, M. Sayeed, S.C. Das, S. Grammatikos, S. Pingky, R. Khan, Development of heavy mineral filler based FRP composites for (low energy) radiation shielding application, *Radiation Effects and Defects in Solids* **179** (9-10) 1132-1152 (2024).
- [17] M. Ozturk, A. Karabulut, Electromagnetic interference shielding properties of carbon fiber mortars with mill scale and red mud: a comparative study, *Construction and Building Materials* **451** 138827 (2024).
- [18] K. Sukhareva, I. Burmistrov, E. Mamin, A. Maltsev, S. Karpova, P.O. Ofkor, Effects of neat and silver coated fly ash cenospheres on the properties of styrene-butadiene-styrene block copolymer composites obtained by a solution mixing method, *Journal of Elastomers & Plastics* **56** (6) 745-773 (2024).
- [19] S.B. Kondawar, P.R. Modak, Theory of EMI shielding, *Materials for Potential EMI Shielding Applications*, Elsevier, pp. **9-25** (2020).
- [20] A.A. Isari, A. Ghaffarkhah, S.A. Hashemi, S. Wuttke, M. Arjmand, Structural design for EMI shielding: from underlying mechanisms to common pitfalls, *Advanced Materials* **36** (24) 2310683 (2024).